Elucidating the Structure and Photophysics of Layered Perovskites through Cation Fluorination

Tekelenburg, Eelco K.; Kahmann, Simon; Kamminga, Machteld E.; Blake, Graeme R.; Loi, Maria A.

Published in:
Advanced optical materials

DOI:
10.1002/adom.202001647

ADVANCED OPTICAL MATERIALS
www.advopticalmat.de

Elucidating the Structure and Photophysics of Layered Perovskites through Cation Fluorination

*Eelco K. Tekelenburg, Simon Kahmann, Machteld E. Kamminga, Graeme R. Blake, and Maria A. Loi**

Optoelectronic devices based on layered perovskites containing fluorinated cations display a well-documented improved stability and enhanced performance over non-fluorinated cations. The effect of fluorination on the crystal structure and photophysics, however, has received limited attention up until now. Here, 3-fluorophenethylammonium lead iodide ($(3\text{-FPEA})_2PbI_4$) single crystals are investigated and their properties to the non-fluorinated ($(PEA)_2PbI_4$) variant are compared. The bulkier 3-FPEA cation increases the distortion of the inorganic layers, resulting in a blue-shifted absorbance and photoluminescence. Temperature-dependent photoluminescence spectroscopy reveals an intricate exciton substructure in both cases. The fluorinated variant shows hot-exciton resonances separated by 12 to 15 meV, values that are much smaller than the 40 to 46 meV found for $(PEA)_2PbI_4$. In addition, high-resolution spectra show that the emission at lower energies consists of a substructure, previously thought to be a single line. With the analysis on the resolved photoluminescence, a vibronic progression is excluded as the origin of the emission at lower energies. Instead, part of the excitonic substructure is proposed to originate from bound excitons. This work furthers the understanding of the photophysics of layered perovskites that has been heavily debated lately.

1. Introduction

Metal halide perovskites have become a popular class of materials due to their outstanding properties for optoelectronic applications. Layered lead iodide perovskites are denoted by the structural formula A_2PbI_4, where A is a large organic cation. The incorporation of such cations results in the formation of inorganic layers sandwiched between the organic cations. Compared to purely 3D perovskites, mixtures of 2D and 3D perovskites have, for example, been incorporated into solar cells and light emitting diodes to improve their ambient and thermal stability as well as their overall performance.[1–4]

It is important to note that improvements in the stability are prerequisites for the use of metal halide perovskites on an industrial scale. The use of layered perovskites in photovoltaic devices has shown important stabilization effects, and in addition, these low dimensional systems are also particularly promising for light-emitting applications. Layered perovskites can be seen as natural quantum wells, where the charge carriers are confined to the inorganic layers. One of the consequences of the confinement is the formation of excitons with binding energies of hundreds of meV.[5,6] The excitonic nature of these materials results in bright and narrow emission, even at room temperature, which enables highly efficient and color-pure LEDs.[7]

In 2019, several reports showed that the use of fluorinated organic cations can further enhance the photovoltaic device performance and stability compared to non-fluorinated cations.[8–11] In addition, halogen-substituted organic cations have shown interesting photophysics, however, more studies are needed to fully understand their physical properties.[12,13]

Several studies on phenethylammonium lead iodide ($(PEA)_2PbI_4$) reported a detailed exciton substructure with multiple photoluminescence (PL) and absorption peaks at cryogenic temperatures.[14,15] The proposed origins vary and include emission from bound excitons,[16,17] vibronic progressions,[13,14] or the formation of distinct exciton polarons.[15,18] The even spacing of the peaks by 40 to 46 meV in both the absorbance and PL spectra was attributed to a single vibronic progression governed by a phonon mode of the organic cation.[14] The energy separation of the peaks could be reduced by substituting different halogens on the phenethylammonium cation, suggesting the importance of a low-energy vibrational mode of the heavier organic cation on the PL structure.[13] However, Thouin et al. reported two distinct exciton polaron peaks, associated with different sets of Raman modes, which excluded the existence of a single vibronic progression.[18] In addition, it was observed that

E. K. Tekelenburg, Dr. S. Kahmann, Dr. M. E. Kamminga, Dr. G. R. Blake, Prof. M. A. Loi
Zernike Institute for Advanced Materials
University of Groningen
Nijenborgh 4, Groningen 9747 AG, The Netherlands
E-mail: m.a.loi@rug.nl
Dr. M. E. Kamminga
Niels Bohr Institute
University of Copenhagen
Universitetsparken 5, Copenhagen Ø DK-2100, Denmark
The ORCID identification number(s) for the author(s) of this article can be found under https://doi.org/10.1002/adom.202001647.

DOI: 10.1002/adom.202001647

the spacing of the peaks, 35 ± 5 meV in their case, was identical in both butylammonium and phenethylammonium layered perovskites, suggesting an overarching mechanism in this class of materials.[15] These recent reports show that no consensus has been reached regarding the origin of these evenly spaced PL peaks.[13,18] With this work we want to contribute to the scientific debate by studying an unexplored fluorinated derivative of phenethylammonium with high spectral resolution.

In this study, the structural and optical properties of 3-fluorophenethylammonium lead iodide ($(3\text{-FPEA})_2PbI_4$) single crystals are investigated and compared to the properties of the prototypical non-fluorinated variant ($(PEA)_2PbI_4$). In both cases, temperature-dependent PL spectra reveal that the emission spectra are dominated by free excitons whose luminescence is broadened by the same effective phonon mode associated with the inorganic cage. High-energy emission from hot-exciton resonances, however, exhibits a smaller separation for the fluorinated variant compared to the prototypical compound. In addition, high-resolution PL spectra at 5.4 K reveal a previously unreported substructure. The diverse spectral shifts and the time-resolved behavior of these PL resonances prove that the peaks do not originate from a single vibronic progression, while excitons bound to defects are their proposed origin.

2. Results

Two types of A_2PbI_4 single crystals, namely 3-fluorophenethylammonium and phenethylammonium lead iodide, were synthesized following the procedure described in our previous work.[19] **Figure** 1a displays the crystal structure of $(3\text{-FPEA})_2PbI_4$ solved in the monoclinic $I2/m$ space group from single crystal X-ray diffraction data collected at 100 K; full details of the structure refinement are given in Table S1, Supporting Information. This structure shows the typical arrangement of alternating organic and inorganic layers found in layered perovskites. The equatorial iodine atoms in the PbI_6 octahedra, depicted by the two-tone white and purple spheres in Figure 1a, show partial occupancies over two positions, which indicate disorder or an unresolved superstructure. The Pb atom also shows partial occupancies over two positions. These occupancies stem from two possible ways that the ammonium group on the 3-FPEA molecule forms hydrogen bonds to the inorganic layer, namely a "pinched-in" or "pinched-out" conformation in the *ab*-plane as previously reported for $(3\text{-FPEA})_2SnI_4$.[20] Furthermore, the mirror plane perpendicular to the *b*-axis results in two partially occupied orientations of the 3-FPEA molecule. We observe evidence for a superstructure with a doubled *b*-axis, as indicated by the weak and rather poorly defined diffraction spots shown in Figure S1, Supporting Information, but this structural model could not be refined in a satisfactory manner. The superstructure might be the result of local ordering of the organic cations, which was reported to be of long-range nature both in the $(3\text{-FPEA})_2PbI_4$ and the $(3\text{-FPEA})_2SnI_4$ crystals.[8,20]

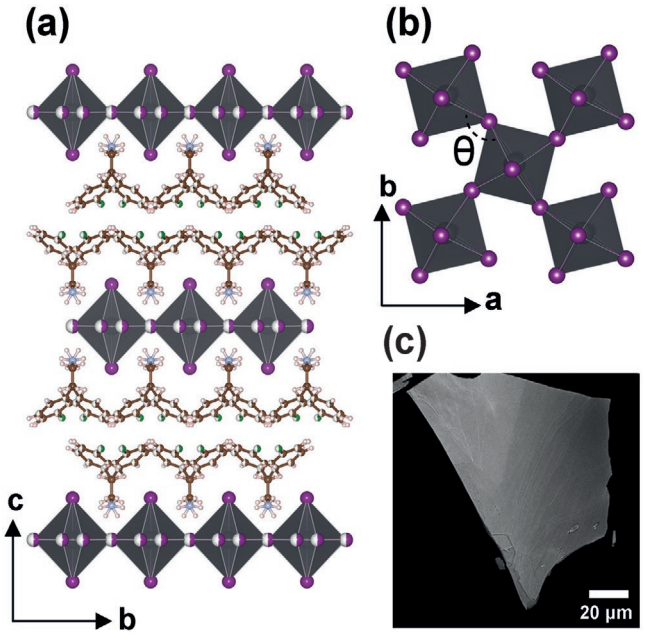

Figure 1. a) $(3\text{-FPEA})_2PbI_4$ crystal structure at 100 K. b) In-plane projection of the inorganic perovskite layer of $(PEA)_2PbI_4$ at 100 K with the Pb–I–Pb angle indicated by θ. c) Confocal PL map of a representative $(3\text{-FPEA})_2PbI_4$ exfoliated crystal.

The structure of $(PEA)_2PbI_4$ at 100 K was solved in the triclinic $P\bar{1}$ space group and exhibits fully ordered octahedral rotations and disordered PEA molecular orientations (Figure 1b and Figure S2, Supporting Information). This results in a basal *ab*-plane that is enlarged by a factor of $a\sqrt{2} \times b\sqrt{2}$ compared to that of $(3\text{-FPEA})_2PbI_4$. The unit cell contains a single inorganic layer and PEA bilayer. This is different to the monoclinic $P21/c$ structure that we previously determined for crystals grown using the antisolvent vapor-assisted method, where both the in-plane octahedral rotations and the orientations of the PEA molecules showed disorder over two positions.[21] It is also different to the monoclinic $C2/m$ structure with disordered rotations reported by Calabrese et al. for crystals grown by a simple solvent evaporation method.[22] Disordered rotations were also reported by Du et al. for crystals grown by a layered-solution method, although with a triclinic $P\bar{1}$ structure with a doubled *c*-axis at room temperature.[23]

The *ab*-plane of $(PEA)_2PbI_4$ is displayed in Figure 1b with the in-plane Pb-I-Pb angle indicated by θ. θ affects the band gap and the photophysics of layered perovskites and is influenced by the choice of the organic cation.[13,24] The bulkier fluorinated cation introduces a larger distortion, decreasing the average θ from 152.24° for $(PEA)_2PbI_4$ to 150.23° for $(3\text{-FPEA})_2PbI_4$. The tilting of the axial iodides is negligible in both materials, indicated by a small distortion up to 1.8°. In addition, the larger 3-FPEA cation introduces a longer interlayer distance, 16.7 Å versus 16.2 Å, in the direction perpendicular to the inorganic layers.

Whereas grain boundaries can influence the properties of multicrystalline thin films, single crystals allow for studying the intrinsic properties of the material. The single crystals were exfoliated in order to obtain clean surfaces. Figure 1c shows the PL map of a representative $(3\text{-FPEA})_2PbI_4$ crystal flake obtained by confocal laser scanning microscopy. As expected from the layered crystal structure, clear step edges are evident as a result of the exfoliation.

Representative PL and absorbance spectra at room temperature are shown in **Figure 2**a for $(3\text{-FPEA})_2PbI_4$ (top) and $(PEA)_2PbI_4$ (bottom). Absorption peaks are located at 2.420 and 2.387 eV for $(3\text{-FPEA})_2PbI_4$ and $(PEA)_2PbI_4$, respectively. The PL for both materials consists of two emission bands: a

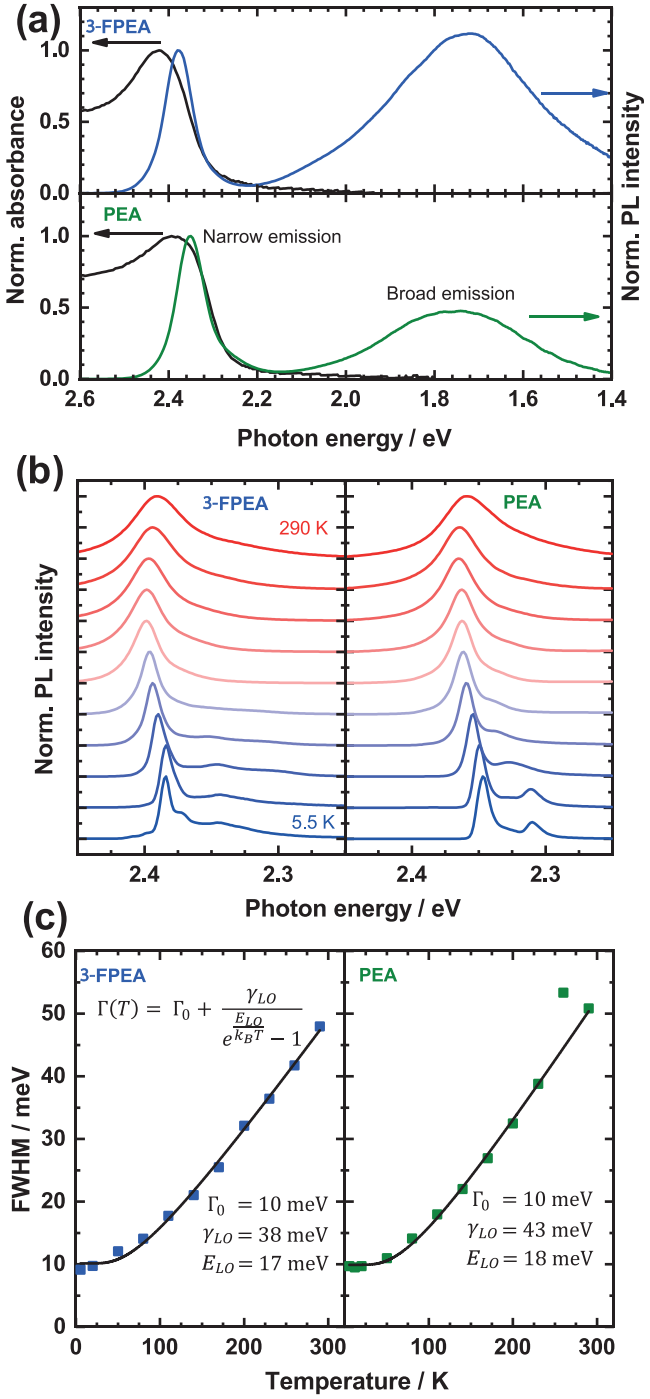

Figure 2. a) The PL and absorbance spectrum of $(3\text{-FPEA})_2PbI_4$ and $(PEA)_2PbI_4$ at room temperature. b) Temperature dependence of the narrow emission for $(3\text{-FPEA})_2PbI_4$ (left) and $(PEA)_2PbI_4$ (right), c) with the FWHMs extracted from Lorentzian fits. The solid line is the fit of the linewidth broadening. The fitted values are indicated in the figure.

narrow emission with peaks at 2.378 and 2.351 eV, and a broad emission with peaks at 1.732 and 1.765 eV for $(3\text{-FPEA})_2PbI_4$ and $(PEA)_2PbI_4$, respectively. Thus, a small Stokes shift of 42 and 36 meV is observed for the narrow emission, and a Stokes shift of hundreds of meV for the broad emission. We previously showed that the broad emission is due to bulk defect states in the band gap, characterized by a longer PL decay compared to the narrow emission; also see Figure S3, Supporting Information.[19] In this report, we aim to provide a deeper understanding of the narrow emission, which is commonly attributed to radiative recombination of free excitons.[25]

A blue shift of 33 meV of the absorption peak is observed with the use of the fluorinated cation compared to the non-fluorinated cation. This shift is attributed predominantly to the larger in-plane distortion in $(3\text{-FPEA})_2PbI_4$, as the larger distortion raises the bottom of the conduction band and lowers the top of the valence band, increasing both the electronic and optical band gap.[24,26]

The asymmetric shape of the narrow emission toward lower energies suggests additional contributions from emitting states, as highlighted in Figure S4, Supporting Information. To verify this assumption, PL spectra were measured as a function of temperature, as shown in Figure 2b. Upon cooling, the narrow emission shows an initial blue shift followed by a red shift starting at 200 K (Figure S5, Supporting Information). This observation is explained by two competing effects: the blue shift is caused by a reduced exciton–phonon interaction, whilst the red shift is caused by the lattice contraction.[27] The lattice contraction increases the overlap of anti-bonding hybridization of Pb 6s and I 5p orbitals of the valence band maximum and the Pb 6p and I5p orbitals of the conduction band, which results in a smaller optical band gap.[26–28] Both materials exhibit a similar behavior of the peak position, suggesting that the difference in distortion and crystal structure does not fundamentally change the behavior of the emission with temperature.

In addition to the shift of the peak position, a narrowing of the PL is observed upon cooling. The main PL peak is fitted with a Lorentzian function, and the full width at half maximum (FWHM) versus temperature is plotted in Figure 2c. Analysis of the PL linewidth can reveal different scattering mechanisms.[15,29–31] The total PL linewidth is typically described by the summation of an inhomogeneous broadening term Γ_0, the scattering by longitudinal optical (LO) and acoustic phonons, and the scattering from ionized impurities:

$$\Gamma(T) = \Gamma_0 + \gamma_{ac}T + \frac{\gamma_{LO}}{e^{\frac{E_{LO}}{k_B T}} - 1} + \gamma_{imp} e^{\frac{-E_{imp}}{k_B T}} \quad (1)$$

where γ_{ac}, γ_{LO} and γ_{imp} are the effective coupling strengths of scattering by acoustic phonons, optical phonons, and ionized impurities, respectively. E_{LO} is the effective optical phonon energy, and E_{imp} is the effective binding energy of ionized impurities. Each of the terms in Equation (1) gives a distinct trend of the linewidth. Figure 2c shows that an excellent fit to the temperature-dependent broadening of the linewidth can be achieved by exclusively considering contributions from LO phonons. Thus, there is negligible contribution of acoustic phonons and ionized impurities to the FWHM, which is consistent with other metal halide perovskites.[2,15,31,32] Therefore, we attribute the dominant broadening to scattering by LO phonons, and their values are displayed in Figure 2c.

Both materials show virtually identical values for the effective phonon energy (17 meV) and phonon coupling strength

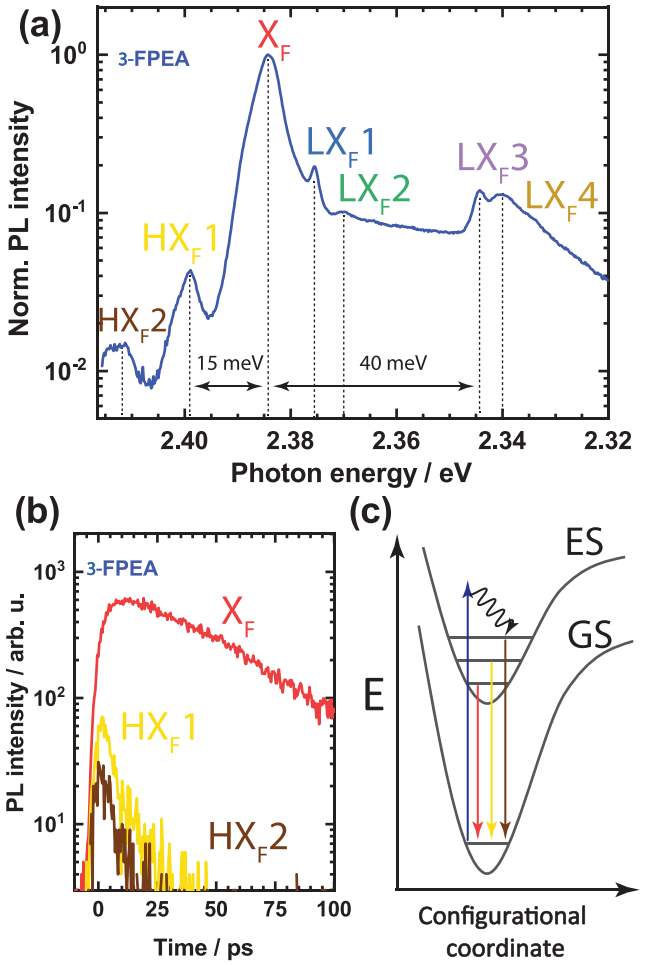

Figure 3. a) The narrow emission of $(3\text{-FPEA})_2PbI_4$ at 5.4 K shows multiple PL peaks both on the high energy side of the free exciton X_F as well as on the low energy side. The HX_F2, HX_F1, and X_F peaks all show a similar high energy shoulder. b) Their time-resolved traces are shown in. c) The recombination processes of HX_F2, HX_F1, and X_F peaks are illustrated in a configurational coordinate scheme with ES being the electronic excited state and GS the ground state.

(≈40 meV), showing that the same phonons are involved in the broadening of the PL. We identify Raman modes at 2.9 meV (23 cm^{-1}), 5.3 meV (43 cm^{-1}), 7.1 meV (57 cm^{-1}), 12.4 meV (100 cm^{-1}), 17.4 meV (140 cm^{-1}), 32.6 meV (263 cm^{-1}), and 51.3 meV (414 cm^{-1}) that could be accounted for the observed effective phonon energy (Figure S6, Supporting Information). Phonon energies up to 17 meV are typically associated with the modes of the lead iodide cage of the perovskites.[14,15,28,31,33,34] To verify this correlation in our materials, we compared the Raman modes of PbI_2 with those of $(3\text{-FPEA})_2PbI_4$ and $(PEA)_2PbI_4$ (Figure S7, Supporting Information). We observed Raman modes up to 20.6 meV (166 cm^{-1}) in PbI_2. This suggests that the low-energy modes up to 17.4 meV are dominated by the lead iodide cage, whilst higher energy modes include Raman contributions of the organic cations.[14,18] The Raman modes that are observed at room temperature play an important role also at low temperature, as shown in Figure S8, Supporting Information.

Table 1. Summary of the energetic positions of the PL peaks.

	HX2	HX1	X	LX1	LX2	LX3	LX4
3-FPEA	2.411 eV	2.399 eV	2.384 eV	2.376 eV	2.371 eV	2.344 eV	2.340 eV
PEA	2.435 eV	2.389 eV	2.349 eV	2.347 eV	2.309 eV	2.305 eV	–

The low-temperature PL spectra in Figure 2b show an intricate peak substructure. To elucidate the nature of those features, we measured high-resolution spectra of the two samples at 5.4 K. We will first discuss the spectrum of $(3\text{-FPEA})_2PbI_4$, which is shown in **Figure 3**a. The most intense peak X_F is attributed to the recombination of free excitons, consistent with its temperature behavior discussed above and its linear dependence on the excitation fluence (Figure S9, Supporting Information). The PL peaks at the high-energy side of the free exciton are denoted as HX_F1 and HX_F2, whilst the peaks at lower energy are LX_F1, LX_F2, LX_F3, and LX_F4. The energetic positions of the above mentioned features are summarized in **Table 1**.

Starting from the high-energy side of the free exciton, HX_F2 and HX_F1 are typically ascribed to hot-exciton emission.[13,14] The peaks are separated by 12 to 15 meV, which is in the region of the phonon modes discussed above. X_F and HX_F1 are both asymmetric with a shoulder at high energy, suggesting an unresolved substructure. We excluded a significant contribution of PbI_2, a known degradation product, to the measured high-energy spectra of the layered perovskites; see Figure S11, Supporting Information.[35]

The time-resolved PL of the peaks HX_F2, HX_F1, and X_F are displayed in Figure 3b. Here, the peaks HX_F2 and HX_F1 show a fast decay with a lifetime of ≈5 ps; the instrumental resolution is approximately 2 to 3 ps. Peak X_F shows a much slower decay of 43 ps. In addition, peak X_F shows a delayed onset of approximately 10 ps, indicating that relaxation occurs from higher energy states toward the bottom of the electronic excited state (ES). The fast decay of peaks HX_F2 and HX_F1 together with their energy spacing coinciding with perovskite phonon modes leads us to ascribe these emissions to the radiative recombination of hot excitons as part of a vibronic progression; this is schematically depicted in Figure 3c.

The low-temperature PL spectrum of $(PEA)_2PbI_4$ also shows high-energy peaks (Figure S12, Supporting Information, peaks HX_P2 and HX_P1) that are in accordance with previous reports.[14,15] Strikingly, the interpeak separation is 40 to 46 meV for $(PEA)_2PbI_4$, therefore much larger than the 12 to 15 meV separation for $(3\text{-FPEA})_2PbI_4$. The smaller energy spacing of 12 to 15 meV in $(3\text{-FPEA})_2PbI_4$ opposes the view that the energy spacing of 35 ± 5 meV is an overarching observation in these materials.[15,36]

Similar to a previous report, we observe that the heavier mass of the halogen reduces the spacing of the hot-exciton emissions.[13] Assuming the hot-exciton peaks originate from a vibronic progression, it is remarkable that there is practically no change of modes observable in the Raman spectra (Figures S6 and S8, Supporting Information). Since Raman spectroscopy only probes the electronic ground state (GS), one explanation would be strikingly different modes in the electronic excited state governed by the organic cation. This observation warrants further studies to explain the impact of fluorination on the vibrational structure of the electronic excited state.

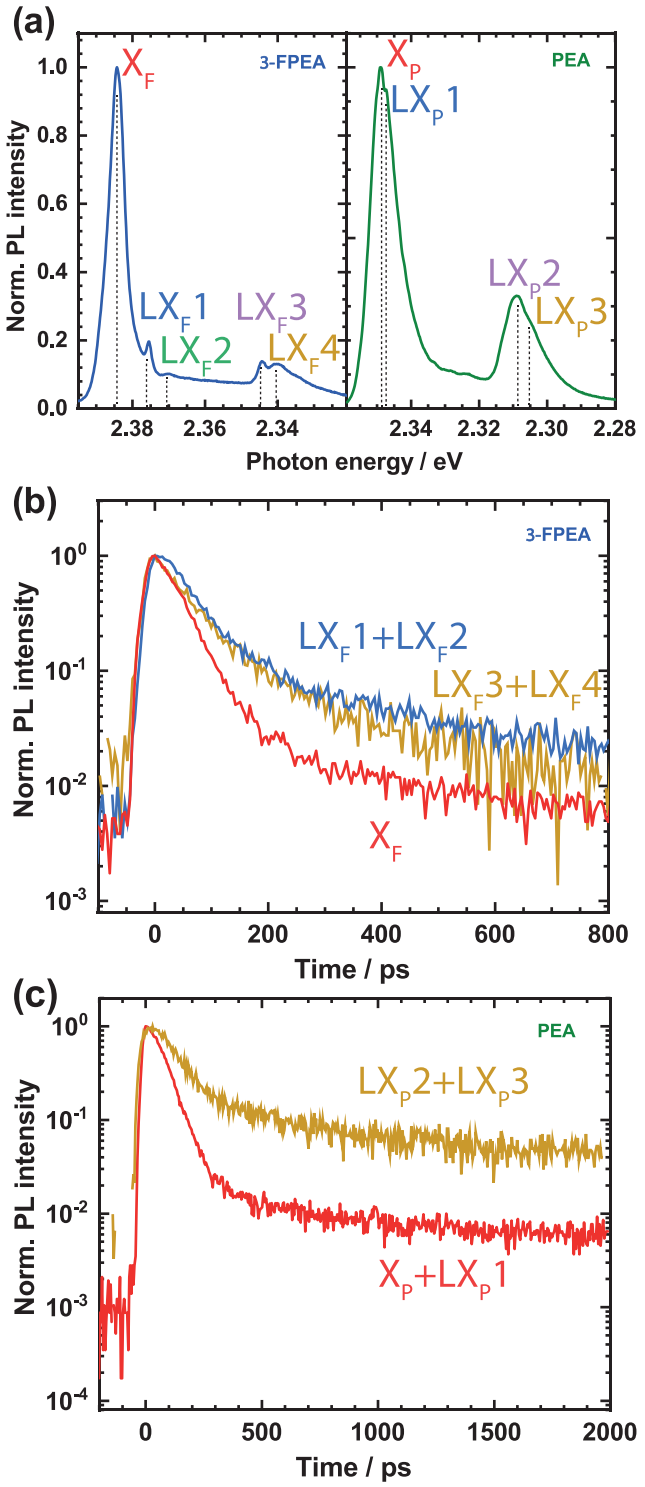

Figure 4. a) Normalized PL spectra of $(3\text{-FPEA})_2PbI_4$ and $(PEA)_2PbI_4$ show similar low-energy substructure. Time-resolved traces of the main peak together with the low-energy peaks b) of $(3\text{-FPEA})_2PbI_4$ and c) of $(PEA)_2PbI_4$.

Focusing on the low-energy side of the free exciton, **Figure 4**a shows a similar substructure in both compounds: LX_F3 and LX_F4 for $(3\text{-FPEA})_2PbI_4$; LX_P2 and LX_P3 for $(PEA)_2PbI_4$. Analogous to the room-temperature PL, the PL at 5.4 K of $(3\text{-FPEA})_2PbI_4$ is shifted to higher energy compared to the PL of $(PEA)_2PbI_4$ due to the increased distortion of the Pb-I-Pb angle. The substructures are only observed using a high-resolution grating. In addition, these high-resolution spectra allow to observe important differences near the main peak, that is, two individual peaks LX_F1 and LX_F2 for $(3\text{-FPEA})_2PbI_4$ and LX_P1 for $(PEA)_2PbI_4$. Mostly, these differences appear from a larger broadening of the PL of $(PEA)_2PbI_4$, which could be determined by a form of long-range disorder characterizing this system. The small rotations of the inorganic layers around the stacking direction observed for this system (see Figure S1, Supporting Information), could be the source of such a disorder. The shoulder LX_P1 could indicate a fine-structure splitting of the free exciton.[21,37] The plateau between LX_F2 and LX_F3 in $(3\text{-FPEA})_2PbI_4$, and between LX_P1 and LX_P2 in $(PEA)_2PbI_4$ indicates emission from a large number of unresolved peaks.

Variation of the excitation fluence can help in discriminating recombination processes from each other. The PL intensity of these processes can be described by $I \propto P^k$ with P the excitation fluence.[38,39] Monomolecular recombination processes, for example, exciton recombination, typically show an exponent k of one. Exponents equal to or lower than one can be linked to free-to-bound and donor–acceptor pair transitions, whereas both a linear and superlinear dependence are associated with bound excitons.[38] A superlinear dependence has also been attributed to the emission of biexcitons in layered perovskites.[21,28,40]

The PL intensities versus increasing excitation fluence are presented in Figure S9, Supporting Information for $(3\text{-FPEA})_2PbI_4$ and Figure S10, Supporting Information for $(PEA)_2PbI_4$. The main peaks X rise linearly with increasing excitation fluence, corroborating our assignment of free exciton emission. Interestingly, peaks LX_F3 and LX_F4 in $(3\text{-FPEA})_2PbI_4$ show a linear dependence opposed to the superlinear dependence of peaks LX_P2 and LX_P3 in $(PEA)_2PbI_4$. This suggests either the absence of biexcitons in $(3\text{-FPEA})_2PbI_4$ or the misattribution of biexcitons in $(PEA)_2PbI_4$, since a superlinear dependence points both to the emission of bound excitons and biexcitons.[21,38]

We extracted the time-resolved traces of the free exciton and the low-energy peaks for both materials, as shown in Figure 4b,c. The traces of the low-energy peaks are combined as these could not be displayed separately; see Figure S13, Supporting Information for the streak camera images. The PL for both materials shows a biexponential decay, where the free exciton decays faster than the low-energy peaks, as summarized in **Table 2**. Additionally, the low-energy traces exhibit a delayed onset up to tens of picoseconds, suggesting a transfer process from the free exciton. The similarity of PL decays of $LX1_F+LX_F2$ and LX_F3+LX_F4 suggests a similar origin of these emissions. We note that a long PL tail of LX_F1+LX_F2 continues well beyond the displayed time window and persists for hundreds of ns into the µs range (Figure S14, Supporting Information). It has been argued that the long decay stems from weakly allowed emission from a dark state due to spin-orbit coupling and intermixing of a triplet state with a singlet state.[21,41,42] This leads us to assume the presence of a dark state slightly below the main peak of $(3\text{-FPEA})_2PbI_4$ as observed in $(PEA)_2PbI_4$; see for additional discussion Note S1, Supporting Information.[21]

As mentioned earlier, the assignment of the low-energy PL peaks in layered perovskites based on PEA has been a source

Table 2. Summary of PL lifetimes.

	X_F	LX_F1+LX_F2	LX_F3+LX_F4	X_P+LX_P1	LX_P2+LX_P3
τ_1	36 ps	48 ps	51 ps	54 ps	85 ps
τ_2	190 ps	265 ps	194 ps	503 ps	593 ps

of contradicting reports.[13–18,43] Explanations include excitons bound to defects,[16,17] vibronic progressions,[13,14,43] and exciton polarons.[15,18]

Our data, namely, the intricate substructure, the PL intensity dependence on the excitation fluence, and the slower PL decay of the low-energy peaks suggests the presence of bound excitons. This explanation is further corroborated by the marked change in PL intensity upon temperature variation, an observation only expected for bound excitons (Figure S15, Supporting Information).[17] It is clear that, as discussed above, the crystal structure influences the emission energy of the of the bound excitons. The larger emission linewidth of X_P compared to X_F could indicate an increased disorder in $(PEA)_2PbI_4$; an example could be the small rotation of the inorganic planes around the stacking direction.

Furthermore, for the emission LX_F3 and LX_F4, we exclude that phonon replicas could be their origin as the required modes in the Raman spectra are absent. In addition, we have no clear evidence of the energetic separation of 35 meV to confirm the proposed model of exciton polarons being important for this class of materials.

3. Conclusion

To conclude, in this study we address a current debate in the literature and contribute to the understanding of the emission properties of layered perovskites. This is achieved by investigating the structural and optical properties of $(3\text{-FPEA})_2PbI_4$ and $(PEA)_2PbI_4$ single crystals. Fluorination of the organic cation increases the distortion of the octahedral layer, resulting in a shift to higher energy of the absorbance and PL spectrum. Interestingly, the PL spectra exhibit an intricate substructure at 5.4 K, where the interpeak separation of two hot-exciton peaks is reduced from 40 to 46 meV for $(PEA)_2PbI_4$ to 12 to 15 meV for $(3\text{-FPEA})_2PbI_4$. In addition, high-resolution PL spectra show a previously unreported substructure in the low-energy peaks. Analysis of these spectra reveals that the emission at lower energies originates from bound excitons, in contrast to the commonly reported phonon replicas.

Supporting Information

Supporting Information is available from the Wiley Online Library or from the author.

Acknowledgements

The authors kindly thank A.F. Kamp and T. Zaharia for their technical support. H. Duim is gratefully acknowledged for his advice on the manuscript as is M.J. Rivera Medina for the preparation of PbI_2 thin films. E.K.T. acknowledges the financial support of the Zernike Institute of Advanced Materials. S.K. is supported by the Deutsche Forschungsgemeinschaft (DFG) for a postdoctoral fellowship (Grant No. 408012143). M.E.K. was supported by The Netherlands Organization for Scientific Research (NWO Graduate Programme 2013, No. 022.005.006). This work was financed through the Materials for Sustainability (Mat4Sus) program (739.017.005) of the Netherlands Organisation for Scientific Research (NWO).

Conflict of Interest

The authors declare no conflict of interest.

Data Availability Statement

Research data are not shared.

Keywords

crystal substructure, fluorinated cations, layered perovskites, luminescence spectroscopy, photophysics, Ruddlesden–Popper phase, single crystals

Received: September 23, 2020
Revised: January 20, 2021
Published online: February 10, 2021

[1] S. Shao, J. Liu, G. Portale, H. H. Fang, G. R. Blake, G. H. ten Brink, L. J. A. Koster, M. A. Loi, *Adv. Energy Mater.* **2018**, *8*, 1702019.
[2] S. Kahmann, S. Shao, M. A. Loi, *Adv. Funct. Mater.* **2019**, *29*, 1902963.
[3] Y. Chen, Y. Sun, J. Peng, J. Tang, K. Zheng, Z. Liang, *Adv. Mater.* **2018**, *30*, 1703487.
[4] A. Rajagopal, K. Yao, A. K. Jen, *Adv. Mater.* **2018**, *30*, 1800455.
[5] T. Ishihara, J. Takahashi, T. Goto, *Phys. Rev. B* **1990**, *42*, 11099.
[6] T. Dammak, M. Koubaa, K. Boukheddaden, H. Bougzhala, A. Mlayah, Y. Abid, *J. Phys. Chem. C* **2009**, *113*, 19305.
[7] A. Fakharuddin, U. Shabbir, W. Qiu, T. Iqbal, M. Sultan, P. Heremans, L. Schmidt-Mende, *Adv. Mater.* **2019**, *31*, 1807095.
[8] J. Hu, I. W. H. Oswald, S. J. Stuard, M. M. Nahid, N. Zhou, O. F. Williams, Z. Guo, L. Yan, H. Hu, Z. Chen, X. Xiao, Y. Lin, Z. Yang, J. Huang, A. M. Moran, H. Ade, J. R. Neilson, W. You, *Nat. Commun.* **2019**, *10*, 1276.
[9] J. Shi, Y. Gao, X. Gao, Y. Zhang, J. Zhang, X. Jing, M. Shao, *Adv. Mater.* **2019**, *31*, 1901673.
[10] Q. Zhou, L. Liang, J. Hu, B. Cao, L. Yang, T. Wu, X. Li, B. Zhang, P. Gao, *Adv. Energy Mater.* **2019**, *9*, 1802595.
[11] Y. Liu, S. Akin, L. Pan, R. Uchida, N. Arora, J. V. Milić, A. Hinderhofer, F. Schreiber, A. R. Uhl, S. M. Zakeeruddin, A. Hagfeldt, M. I. Dar, M. Grätzel, *Sci. Adv.* **2019**, *5*, eaaw2543.
[12] D. B. Straus, N. Iotov, M. R. Gau, Q. Zhao, P. J. Carroll, C. R. Kagan, *J. Phys. Chem. Lett.* **2019**, *10*, 1198.
[13] D. B. Straus, S. Hurtado Parra, N. Iotov, Q. Zhao, M. R. Gau, P. J. Carroll, J. M. Kikkawa, C. R. Kagan, *ACS Nano* **2020**, *14*, 3621.
[14] D. B. Straus, S. Hurtado Parra, N. Iotov, J. Gebhardt, A. M. Rappe, J. E. Subotnik, J. M. Kikkawa, C. R. Kagan, *J. Am. Chem. Soc.* **2016**, *138*, 13798.
[15] S. Neutzner, F. Thouin, D. Cortecchia, A. Petrozza, C. Silva, A. R. Srimath Kandada, *Phys. Rev. Materials* **2018**, *2*, 64605.
[16] W. K. Chong, K. Thirumal, D. Giovanni, T. W. Goh, X. Liu, N. Mathews, S. Mhaisalkar, T. C. Sum, *Phys. Chem. Chem. Phys.* **2016**, *18*, 14701.

[17] N. Kitazawa, M. Aono, Y. Watanabe, *Mater. Chem. Phys.* **2012**, *134*, 875.
[18] F. Thouin, D. A. Valverde-Chávez, C. Quarti, D. Cortecchia, I. Bargigia, D. Beljonne, A. Petrozza, C. Silva, A. R. Srimath Kandada, *Nat. Mater.* **2019**, *18*, 349.
[19] S. Kahmann, E. K. Tekelenburg, H. Duim, M. E. Kamminga, M. A. Loi, *Nat. Commun.* **2020**, *11*, 2344.
[20] D. B. Mitzi, C. D. Dimitrakopoulos, L. L. Kosbar, *Chem. Mater.* **2001**, *13*, 3728.
[21] H.-H. Fang, J. Yang, S. Adjokatse, E. K. Tekelenburg, M. E. Kamminga, H. Duim, J. Ye, G. R. Blake, J. Even, M. A. Loi, *Adv. Funct. Mater.* **2020**, *30*, 1907979.
[22] J. Calabrese, N. Jones, R. Harlow, N. Herron, D. Thorn, Y. Wang, *J. Am. Chem. Soc.* **1991**, *113*, 2328.
[23] K. Z. Du, Q. Tu, X. Zhang, Q. Han, J. Liu, S. Zauscher, D. B. Mitzi, *Inorg. Chem.* **2017**, *56*, 9291.
[24] J. L. Knutson, J. D. Martin, D. B. Mitzi, *Inorg. Chem.* **2005**, *44*, 4699.
[25] D. B. Straus, C. R. Kagan, *J. Phys. Chem. Lett.* **2018**, *9*, 1434.
[26] J. Even, L. Pedesseau, M. A. Dupertuis, J. M. Jancu, C. Katan, *Phys. Rev. B* **2012**, *86*, 3.
[27] S. Wang, J. Ma, W. Li, J. Wang, H. Wang, H. Shen, J. Li, J. Wang, H. Luo, D. Li, *J. Phys. Chem. Lett.* **2019**, *10*, 2546.
[28] F. Thouin, S. Neutzner, D. Cortecchia, V. A. Dragomir, C. Soci, T. Salim, Y. M. Lam, R. Leonelli, A. Petrozza, A. R. S. Kandada, C. Silva, *Phys. Rev. Materials* **2018**, *2*, 34001.
[29] S. Rudin, T. L. Reinecke, *Phys. Rev. B* **1990**, *41*, 3017.
[30] J. Lee, E. S. Koteles, M. O. Vassell, *Phys. Rev. B* **1986**, *33*, 5512.
[31] A. D. Wright, C. Verdi, R. L. Milot, G. E. Eperon, M. A. Pérez-Osorio, H. J. Snaith, F. Giustino, M. B. Johnston, L. M. Herz, *Nat. Commun.* **2016**, *7*, 11755.
[32] H. H. Fang, F. Wang, S. Adjokatse, N. Zhao, J. Even, M. A. Loi, *Light: Sci. Appl.* **2016**, *5*, e16056.
[33] K. Gauthron, J.-S. Lauret, L. Doyennette, G. Lanty, A. A. Choueiry, S. Zhang, A. Brehier, L. Largeau, O. Mauguin, J. Bloch, E. Deleporte, *Opt. Express* **2010**, *18*, 5912.
[34] M. Baranowski, S. J. Zelewski, M. Kepenekian, B. Traoré, J. M. Urban, A. Surrente, K. Galkowski, D. K. Maude, A. Kuc, E. P. Booker, R. Kudrawiec, S. D. Stranks, P. Plochocka, *ACS Energy Lett.* **2019**, *4*, 2386.
[35] H. H. Fang, J. Yang, S. Tao, S. Adjokatse, M. E. Kamminga, J. Ye, G. R. Blake, J. Even, M. A. Loi, *Adv. Funct. Mater.* **2018**, *28*, 1800305.
[36] A. R. Srimath Kandada, C. Silva, *J. Phys. Chem. Lett.* **2020**, *11*, 3173.
[37] T. T. H. Do, A. G. del Águila, D. Zhang, J. Xing, S. Liu, M. A. Prosnikov, W. Gao, K. Chang, P. C. M. Christianen, Q. Xiong, *Nano Lett.* **2020**, *20*, 5141.
[38] T. Schmidt, K. Lischka, W. Zulehner, *Phys. Rev. B* **1992**, *45*, 8989.
[39] I. Pelant, J. Valenta, *Luminescence of Excitons*, Oxford University Press, Oxford **2012**.
[40] T. Kondo, T. Azuma, T. Yuasa, R. Ito, *Solid State Commun.* **1998**, *105*, 253.
[41] K. Tanaka, T. Takahashi, T. Kondo, K. Umeda, K. Ema, T. Umebayashi, K. Asai, K. Uchida, N. Miura, *Jpn. J. Appl. Phys., Part 1* **2005**, *44*, 5923.
[42] K. Ema, M. Inomata, Y. Kato, H. Kunugita, M. Era, *Phys. Rev. Lett.* **2008**, *100*, 257401.
[43] J. M. Urban, G. Chehade, M. Dyksik, M. Menahem, A. Surrente, G. Trippé-Allard, D. K. Maude, D. Garrot, O. Yaffe, E. Deleporte, P. Plochocka, M. Baranowski, *J. Phys. Chem. Lett.* **2020**, *11*, 5830.